Interference Effects in Sum Frequency Spectra from Monolayers on Composite Dielectric/Metal Substrates

Alex G. Lambert, David J. Neivandt,[†] Adam M. Briggs,[‡] Eric W. Usadi,[§] and Paul B. Davies*

Department of Chemistry, University of Cambridge, Lensfield Road, Cambridge, CB2 1EW, U.K.

Received: November 15, 2001; In Final Form: January 9, 2002

A theoretical model has been developed to describe the generation of Sum Frequency (SF) light from a monolayer film adsorbed to the surface of a dielectric and metal composite substrate. This type of substrate provides enhanced SF signals from the monolayer without modifying the intrinsic (hydrophilic) properties of the dielectric surface. The fundamental equations of both resonant and nonresonant SF generation have been extended from a single interface to encompass the two displaced sources, the air/dielectric interface at which the monolayer film is located, and the dielectric/metal interface. The model describes the coherent addition of three separate SF signals which coherently interfere with each other, thereby affecting the line-shape observed in the net SF spectrum. Representative calculations have been made for a highly ordered monolayer of an aliphatic hydrocarbon molecule, adsorbed on a dielectric with the optical properties of mica, which is itself in contact with a metal modeled to resemble gold. The SF spectral line-shapes are predicted as a function of the thickness of the dielectric material for the methyl terminal groups of the hydrocarbon chain. The model can be applied to any dielectric/metal composite by modifying the optical properties appropriately.

Introduction

Hydrophilic surfaces such as cotton, enamel, and mineral oxides which are widespread in nature are of great interest due to the diverse industrial processes that rely on adsorption or interaction with them. Deeper insight into the fundamental aspects of adsorption at hydrophilic surfaces is commonly hampered by interfacial heterogeneity, irregular morphology, or cleanliness considerations. For a majority of naturally occurring organic materials such as cotton, only the more rudimentary surface characterization techniques, for example, friction measurements and contact angle determinations have proven useful. To gain a better understanding requires simpler, reproducible hydrophilic substrates such as silica, alumina, or mica and compatible techniques to study them.

The nonlinear optical technique of Sum Frequency vibrational Spectroscopy (SFS) is a proven method for investigating the structure of monolayers adsorbed to optically flat surfaces.[1−4] Although early SF spectrometers typically incorporated nanosecond laser systems, both picosecond and femtosecond spectrometers are now commonly employed. Whilst nanosecond SF spectrometers are less sensitive than their pico and femtosecond counterparts they still provide a significant contribution to published literature and are valued for their reliability and ease of use. Recent work to increase the sensitivity of nanosecond SF systems and hence improve their applicability has centered on using total internal reflection (TIR) beam geometries.[5] A signal enhancement of several orders of magnitude has been reported[6] and originates from the imaginary values of the Fresnel factors at the critical TIR geometry.[7] A simpler, but equally effective method of increasing the SF signal from molecules adsorbed at an interface is to employ a substrate that can itself generate a significant SF signal.[2,8] Thus, adsorption at a hydrophobic surface has been extensively studied using a model (hydrophobic) layer of self-assembled per-deuterated alkanethiol adsorbed to a gold substrate.[9] Gold has a strong interband electronic transition in the visible region of the electromagnetic spectrum which is excited by the incident visible beam in a SF experiment. The resulting surface plasmon resonance generates a significant substrate SF signal that amplifies the weaker adsorbate SF emission through coherent optical interference. An additional advantage of using a metal such as gold as a substrate is that the phase difference between the substrate and the adsorbate signals is immediately apparent from the line shapes in the SF spectra, allowing the net polar orientation of the adsorbate species to be determined with ease.[2,9]

Although the metal substrate methodology has proved invaluable for the study of hydrophobic surfaces, its application to the study of adsorption at hydrophilic surfaces has been less successful.[10] The reasons for this are that a hydrophilically functionalized alkanethiol monolayer is not a satisfactory analogue for either the chemical functionality or morphology of industrial hydrophilic surfaces. In addition, recent work has highlighted the significant solvent induced structural changes that can occur with hydrophilically terminated alkanethiol monolayers.[11−14] A facile alternative to functionalized alkanethiol monolayers is freshly deposited gold. However, this surface is also an unsatisfactory hydrophilic mimic, not only in functionality and morphology, but also because it rapidly becomes hydrophobic under ambient conditions. More stable hydrophilic materials, such as the mineral oxides, are of greater practical application, particularly in the case of mica where fresh surfaces may easily be obtained by cleaving along the natural crystallographic planes.[15] However, mineral oxides are dielectrics, lacking electronic and vibrational transitions in the electromagnetic spectrum probed by SFG. They are therefore

---

* To whom correspondence should be addressed. Tel: +44 1223 336460. Fax: +44 1223 336362. E-mail: PBD2@cam.ac.uk.
† Department of Chemical Engineering, The University of Maine, Orono, Maine, 04469, USA.
‡ Lever Faberge, 3 St James's Road, Kingston upon Thames, Surrey, KT1 2BA, U.K.
§ National Physical Laboratory, Queens Road, Teddington, Middlesex, TW11 0LW, U.K.

incapable of forming surface plasmon waves which give rise to the substrate SF signal. Without a substrate SF signal, the intensity of resonant modes from adsorbates on hydrophilic dielectric surfaces are particularly weak.

In 1997, Briggs et al.[16] showed that substantial enhancement of the resonant sum frequency signal from a monolayer on a hydrophilic surface could be achieved by coating the reverse side of a thin dielectric sheet with metal. An interference effect between the SF signal generated from the dielectric/metal interface and the resonant signal generated by a monolayer at the dielectric/air interface was observed if the dielectric was optically transmitting in the appropriate wavelength regions and was of the order of micrometers in thickness. This composite surface technique was subsequently used to study the chemistry and adsorption at a dielectric surface,[15] while benefiting from the high signal levels and orientational information obtained from a metal surface such as gold. This type of composite substrate is equally applicable to picosecond SF systems, providing not only increased signal levels and orientational information, but also the possibility of probing power sensitive monolayers at lower incident beam energies. However, from the initial work of Briggs et al.,[16] it was predicted that the lineshapes observed in the SF spectrum from a monolayer adsorbed to a composite substrate would be dependent upon the thickness of the dielectric material. To obtain an accurate interpretation of the spectra, this behavior requires quantitative modeling.

Spectral modeling is an essential aspect of the interpretation of experimental SF spectra and several models and theoretical descriptions of SFG have appeared in the literature.[7,17−20] However, these models typically describe only a single interface at which a vibrationally active monolayer is located.[18,19] A considerably greater level of sophistication is needed to describe SF generation in the composite air/dielectric/metal system considered in this work. The most closely related SF modeling study to that reported here is by Hirose and co-workers[21,22] for simulating the SF signal produced during the growth of multiple formic acid layers on a Pt(111) surface. Each molecular layer was regarded as a source of SF generation and phase/distance relationships were considered in this work, although only the formic acid layers themselves were perceived to be SF active.[21] This is in contrast to the single resonantly SF active monolayer separated from a nonresonantly SF active metal surface by a transmitting but SF inactive dielectric material as in the experiment of Briggs et al.[16] The aim of this article is to provide a quantitative description of SF generation from species adsorbed on this type of composite dielectric/metal substrate. In turn, this should provide predictions of the dielectric thickness/resonant line-shape behavior and consequently allow unambiguous interpretation of experimental spectra.

The Composite Substrate Model

The intensity of SF light generated at an interface and incident upon a detector is dependent not only upon the SF response from the adsorbate and substrate, but also on experimental parameters such as the beam powers, the overlap integral of the surface electric fields and the detector efficiency.[2] The SF model presented here is designed to predict the former, namely the relative spectral features that arise from coherent interference between the signal from the adsorbate and that from the displaced substrate. Within this premise, it is possible to model the SF signal from a composite substrate by considering the relationships between each of the distinct sources of SF light. In addition, it is important to appreciate that it is only possible to model a comparatively elementary description of the com-
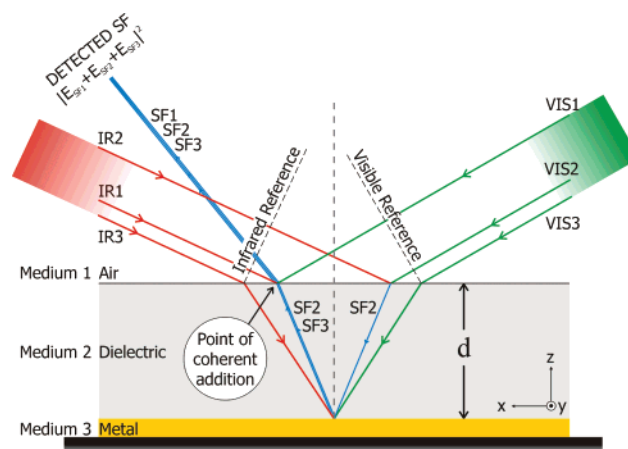

Figure 1. Schematic diagram of the composite dielectric/metal substrate. The incident infrared and visible beams along with their corresponding planes of reference are shown. The three sum frequency beams generated are indicated, as is the point of coherent addition.

posite substrate. First, a three-layered description of the substrate is employed (air/dielectric/metal), and the adsorbed monolayer is considered to be an integral part of the air/dielectric interface. Second, the dielectric component of the composite surface is assumed to be of constant thickness, atomically flat and to be composed of a material with a single wavelength-dependent refractive index. Finally, local field corrections are disregarded, and the possibility of multiple reflections within the thin film dielectric layer are ignored. This latter assumption has been investigated in the present study by modifying the composite substrate model to include multi-reflections. Their inclusion, however, leads to a deterioration in the quality of the experimental comparison over that of the single reflection model presented here.[10] Comparisons of the observed and modeled interference effect will appear in a later paper.

Because the aim of the model is to account for the spectral features generated by the optical interference between multiple SF signals an important aspect is therefore its capacity to determine the relative phase of each of the SF beams at the point of coherent addition. The phase of each of the SF beams can be calculated from the phase change on propagation of the incident beams (visible and infrared), the phase change on SF generation and finally, the phase change as the SF beams propagate to the point of coherent addition. The propagation calculations are based on the schematic ray diagram of the air/ dielectric/metal interface shown in Figure 1. The SF signal generated from the composite substrate is described in terms of a counter-propagating incident beam geometry with three distinct SF sources, two from the adsorbate (SF1 and SF2) and one from the substrate (SF3). The adsorbate SF signal SF1 is generated by the visible beam VIS1 and the infrared beam IR1 at the air/dielectric interface and propagates away from the surface. The adsorbate SF signal SF2 is also generated at the air/dielectric interface by VIS2 and IR2, but unlike SF1, it propagates into the dielectric where it reflects off the dielectric/ metal interface before refracting into air through the dielectric/ air interface. The substrate SF signal, SF3, is generated at the dielectric/metal interface by the visible beam component VIS3 and the infrared beam component IR3; it refracts into air through the dielectric/air interface. The three SF beams in Figure 1 are all parallel to each other as they propagate away from the surface, a strict requirement for coherent addition. Coherent addition is considered to occur at the point at which the path of the beams first coincide, Figure 1. Propagation distances for

Interference Effects in Sum Frequency Spectra

J. Phys. Chem. B, Vol. 106, No. 21, 2002 **5463**

infrared and visible beams prior to the points of SF generation are calculated relative to the two reference planes of common phase, which are perpendicular to the direction of beam propagation and are located arbitrarily.

The single layer of molecules responsible for the resonant adsorbate SF signals (SF1 and SF2) at the air/dielectric interface is assumed to be isotropic and to consist of an aliphatic hydrocarbon chain in an all-trans configuration terminated by a methyl group oriented away from the interface.[23] The resonant SF response from this layer is modeled in terms of the second-order nonlinear susceptibility tensor, $\chi^{(2)}$ following the method published by several authors.[2,18,19,24,25] In contrast to the well-developed understanding of SF generation from hydrocarbon monolayers, rather less is known about nonresonant SF generation from metal surfaces (SF3). Several quite different phenomenological approaches have been adopted in the literature from simply assuming that the substrate SF signal arises from the same components of the susceptibility as the resonant signal[24,26] to considering that SFG from gold occurs from electrons bound just below the gold surface.[27] Conversely, theoretical investigations have attributed metal SFG to surface plasmon resonance and have thus considered solely the $\chi^{(2)}_{zzz}$ component. (Liebsch[28] has employed time-dependent local density approximations to describe SFG from gold, whereas Mendoza[29,30] has developed a complex mathematical model to describe the nonlinear response of the surface in terms of free jellium electrons and bound inter-band electrons). With no current universal agreement, the model developed in this work avoids any assumed specific susceptibility and simply describes the SF signal generated at the dielectric/metal interface as being equal in magnitude and phase along the principal axes.

Calculation Details

(A) Sum Frequency Intensities−ppp Polarization Combination. The equations below were used to simulate the sum frequency emission from the composite substrate when using a ppp beam polarization combination. The particular molecular vibration under consideration need not be specified as the differences between them lie simply in the values of the nonlinear susceptibilities, which are considered later. Because only relative intensities of the SF signals are modeled, the intensity of the SF signal emitted from the composite substrate is related to the p polarized SF E field at the point of coherent addition by

$$I_{p,SF} = I_{x,SF} + I_{z,SF}$$

$$= |\mathbf{E}^{Total}_{x,SF}|^2 + |\mathbf{E}^{Total}_{z,SF}|^2$$

$$= |\mathbf{E}_{x,SF1} + \mathbf{E}_{x,SF2} + \mathbf{E}_{x,SF3}|^2 + |\mathbf{E}_{z,SF1} + \mathbf{E}_{z,SF2} + \mathbf{E}_{z,SF3}|^2 \quad (1)$$

where the x or z SFi subscript refers to the relevant axial component of the ith SF beam of Figure 1. For the resonant SF signals, SF1 and SF2, the emitted electric fields are related to the induced SF polarizations through the SF Fresnel factors (L or so-called "nonlinear" factors) originally derived by Heinz[31] and first published by Hirose.[19] The L factors are given in the Supporting Information with sign adjustments appropriate to the alternative beam geometry and axis system employed in this work. The constants in the L factor equations have been omitted, as only the trigonometric components of the L factor equations are relevant for relative intensities.

Initially, considering purely SF1

$$\mathbf{E}_{x,SF1} = L^R_x \mathbf{P}^{(2)}_{x,SF1} \quad (2)$$

$$\mathbf{E}_{z,SF1} = L^R_z \mathbf{P}^{(2)}_{z,SF1} \quad (3)$$

where $\mathbf{P}^{(2)}_{x,SF1}$ and $\mathbf{P}^{(2)}_{z,SF1}$ are the induced second order nonlinear polarizations at the interface. A complete description of the induced SF polarization at an interface should typically include 9 components of the nonlinear susceptibility for each axial polarization under consideration (27 in total or 18 for p polarized SF, 9 for s polarized SF). However, under the symmetry constraints imposed by a surface with $C_{\infty v}$ symmetry only 7 of the possible 27 components of $\chi^{(2)}_{ijk}$ are nonzero, 4 applicable to p polarized SF light and 3 to s polarized SF light. For SF1, the induced polarizations are given by

$$\mathbf{P}^{(2)}_{x,SF1} = (\chi_{xxz}^{(2)}K_{x,VIS}K_{z,IR} + \chi_{xzx}^{(2)}K_{z,VIS}K_{x,IR})e^{i(\Delta_{IR1}+\Delta_{VIS1})} \quad (4)$$

$$\mathbf{P}^{(2)}_{z,SF1} = (\chi_{zzz}^{(2)}K_{z,VIS}K_{z,IR} + \chi_{zxx}^{(2)}K_{x,VIS}K_{x,IR})e^{i(\Delta_{IR1}+\Delta_{VIS1})} \quad (5)$$

where K_j and K_k are the linear Fresnel coefficients relating the amplitude of the incident beam in air to the amplitude at the interface (Braun et al.[32] and Supporting Information), Δ_{IR1} and Δ_{VIS1} are propagation distance/phase terms of the incident beams described later and $\chi^{(2)}_{ijk}$ are the nonzero components of the second-order susceptibility under $C_{\infty v}$ symmetry constraints. The equations for the nonzero components of $\chi^{(2)}_{ijk}$ are discussed later. The constant terms in the induced polarization equation, specifically ϵ_0, may again be omitted.

The equations for SF2 relating the emitted SF electric field at the point of coherent addition to the induced second-order nonlinear polarization at the interface are similar in form to those of SF1, but include extra propagation distance/phase terms. In addition, transmitting rather than reflecting L factor equations are employed and linear Fresnel reflection (r) and transmission (t) coefficients are required to describe the SF beam reflecting off the dielectric/metal (2/3) interface and refracting through the dielectric/air interface (2/1)

$$\mathbf{E}_{x,SF2} = L^T_x \mathbf{P}^{(2)}_{x,SF2}(r_{p23}t_{p21}e^{i\Delta_{SF2}}) \quad (6)$$

$$\mathbf{E}_{z,SF2} = L^T_z \mathbf{P}^{(2)}_{z,SF2}(r_{p23}t_{p21}e^{i\Delta_{SF2}}) \quad (7)$$

The equations for the induced SF polarization for SF2 are exactly analogous to those for SF1, specifically

$$\mathbf{P}^{(2)}_{x,SF2} = (\chi_{xxz}^{(2)}K_{x,VIS}K_{z,IR} + \chi_{xzx}^{(2)}K_{z,VIS}K_{x,IR})e^{i(\Delta_{IR2}+\Delta_{VIS2})} \quad (8)$$

$$\mathbf{P}^{(2)}_{z,SF2} = (\chi_{zzz}^{(2)}K_{z,VIS}K_{z,IR} + \chi_{zxx}^{(2)}K_{x,VIS}K_{x,IR})e^{i(\Delta_{IR2}+\Delta_{VIS2})} \quad (9)$$

As discussed previously the metal substrate SF E field, SF3, is described in terms of a single magnitude and phase and does not contain a polarization dependence, susceptibility components, or a linear Fresnel factor for the dielectric/air interface. It is, however important to include the propagation phase terms for IR3, VIS3, and the resultant SF3 beam. At the point of coherent interference SF3 is given by

$$\mathbf{E}^{SF3}_{x,SF} \equiv \mathbf{E}^{SF3}_{z,SF} = |E_{NR}|e^{i(\epsilon+\Delta_{IR3}+\Delta_{VIS3}+\Delta_{SF3})} \quad (10)$$

where $|E_{NR}|$ and ϵ are the magnitude and phase respectively of the substrate SF signal as given in Table 1.

TABLE 1: Parameters Employed in the Simulations[a]

parameter	value	parameter	value
$\theta_{1,\text{VIS}}$	60°	n_1	1
$\theta_{1,\text{IR}}$	65°	$n_{2,\text{IR}}$	1.65
λ_{VIS}	532 nm	$n_{2,\text{VIS}}$	1.60
ω_{IR}	2800−3000 cm^{-1}	$n_{2,\text{SF}}$	1.63
ω_ν	2878 cm^{-1}	$n_{3,\text{SF}}$	1.42 + 1.84i
Γ	4 cm^{-1}	n_{layer}	1.18
κ	21°	r	2.5
ξ	34.5°	ϵ(ppp)	initially set to 90° optimized to 169°
		ϵ(ssp)	optimized to 0°
		$|E_{\text{NR}}|$	initially set to 1 optimized to 0.3.

[a] The numerical values are based on a dielectric/metal substrate of mica/gold and a fully trans conformation hydrocarbon monolayer probed in the C−H stretching region by a SF spectrometer built around a frequency doubled nsec Nd:YAG laser.

(B) Sum Frequency Intensities−ssp Polarization Combination. Modification of the model to account for the ssp rather than the ppp beam polarization combination is straightforward. Only one set of SF E fields needs to be considered, namely those along the y axis (Figure 1). The ssp modeling equations are

$$I_{\text{s,SF}} = I_{y,\text{SF}} = |\mathbf{E}_{y,\text{SF1}} + \mathbf{E}_{y,\text{SF2}} + \mathbf{E}_{y,\text{SF3}}|^2 \quad (11)$$

$$\mathbf{E}_{y,\text{SF1}} = L_y^R \mathbf{P}_{y,\text{SF1}}^{(2)} \quad (12)$$

$$\mathbf{E}_{y,\text{SF2}} = L_y^T \mathbf{P}_{y,\text{SF2}}^{(2)} (r_{s23} t_{s21} e^{i\Delta_{\text{SF2}}}) \quad (13)$$

$$\mathbf{E}_{y,\text{SF}}^{\text{SF3}} = |E_{\text{NR}}| e^{i(\epsilon + \Delta_{\text{IR3}} + \Delta_{\text{VIS3}} + \Delta_{\text{SF3}})} \quad (14)$$

$$\mathbf{P}_{y,\text{SF1}}^{(2)} = (\chi_{yyz}^{(2)} K_{y,\text{VIS}} K_{z,\text{IR}} + \chi_{yzy}^{(2)} K_{z,\text{VIS}} K_{y,\text{IR}}) e^{i(\Delta_{\text{IR1}} + \Delta_{\text{VIS1}})} \quad (15)$$

$$\mathbf{P}_{y,\text{SF2}}^{(2)} = (\chi_{yyz}^{(2)} K_{y,\text{VIS}} K_{z,\text{IR}} + \chi_{yzy}^{(2)} K_{z,\text{VIS}} K_{y,\text{IR}}) e^{i(\Delta_{\text{IR2}} + \Delta_{\text{VIS2}})} \quad (16)$$

(C) Susceptibility Components and Phase Factors. Although the above equations can be used to describe the composite substrate interference phenomenon irrespective of molecular vibration, the aim of the present work is to simulate the spectral resonances obtained from a well-packed hydrocarbon layer, namely the r^+, r_{FR}^+, and r^- vibrational modes of the terminal methyl group. The second-order nonlinear susceptibility equations for an r^+ methyl symmetric stretching mode in an isotropic monolayer can be deduced from symmetry considerations but have also been published elsewhere[20,24,25] and are reproduced below for convenience. The Fermi resonance of the symmetric stretching mode must have the same symmetry as the vibrational mode from which intensity is borrowed and, hence, can be modeled with identical $\chi_{ijk}^{(2)}$'s. Because the surface is considered to possess $C_{\infty\nu}$ symmetry, $x \equiv y$ and the r^+ and r_{FR}^+ response to both the ssp and ppp polarization combination can be described using

$$\chi_{zzz}^{(2)} = \frac{[\langle\cos\theta\rangle(3 + R) - \langle\cos3\theta\rangle(R - 1)]}{4(\omega_\nu - \omega_{\text{IR}} - i\Gamma)} \quad (17)$$

$$\chi_{xxz}^{(2)} \equiv \chi_{yyz}^{(2)} = \frac{[\langle\cos\theta\rangle(1 + 7R) + \langle\cos3\theta\rangle(R - 1)]}{8(\omega_\nu - \omega_{\text{IR}} - i\Gamma)} \quad (18)$$

$$\chi_{xzx}^{(2)} \equiv \chi_{yzy}^{(2)} = \chi_{zxx}^{(2)} \equiv \chi_{zyy}^{(2)} = \frac{[\langle\cos\theta\rangle(1 - R) + \langle\cos3\theta\rangle(R - 1)]}{8(\omega_\nu - \omega_{\text{IR}} - i\Gamma)} \quad (19)$$

Only relative intensities are calculated in the model and the parameters β_{ccc} and ϵ_0 that are common to each susceptibility equation have therefore been omitted. R is the hyperpolarizability ratio $\beta_{\text{aac}}/\beta_{\text{ccc}}$, ω_{IR} the tunable infrared frequency, ω_ν the vibrational resonance frequency and Γ^{-1} the relaxation time of the vibrationally excited state. Numerical values for these constants are discussed later and summarized in Table 1. The nonlinear susceptibility equations for the asymmetric methyl stretching mode (r^-) are similar in form to those of the symmetric mode and can be deduced directly from symmetry considerations but have also been published previously.[20,24,25] The $\chi_{ijk}^{(2)}$'s for the r^- mode are

$$\chi_{zzz}^{(2)} = \frac{\langle\cos\theta\rangle - \langle\cos3\theta\rangle}{2(\omega_\nu - \omega_{\text{IR}} - i\Gamma)} \quad (20)$$

$$\chi_{xxz}^{(2)} \equiv \chi_{yyz}^{(2)} = -\frac{\langle\cos\theta\rangle - \langle\cos3\theta\rangle}{4(\omega_\nu - \omega_{\text{IR}} - i\Gamma)} \quad (21)$$

$$\chi_{xzx}^{(2)} \equiv \chi_{yzy}^{(2)} = \chi_{zxx}^{(2)} \equiv \chi_{zyy}^{(2)} = \frac{3\langle\cos\theta\rangle + \langle\cos3\theta\rangle}{4(\omega_\nu - \omega_{\text{IR}} - i\Gamma)} \quad (22)$$

For both the r^+ and the r^- susceptibility equations the average angular distributions between the molecular c axis of the methyl subunit and the surface normal ($\langle\cos\theta\rangle$ and $\langle\cos3\theta\rangle$) can be calculated from the average angle between the hydrocarbon chain and the surface normal (κ) and the angle between the methyl c axis and the hydrocarbon chain axis (ξ) using the method published by Braun et al.,[32] specifically

$$\langle\cos\theta\rangle = \cos\kappa\cos\xi \quad (23)$$

$$\langle\cos3\theta\rangle = \cos\kappa\cos\xi(3\cos2\kappa\cos2\xi - 2\cos^2\kappa\cos^2\xi) \quad (24)$$

Phase variations with propagation distance for both incident and emitted beams are an integral part of the model and are calculated using

$$\Delta = \frac{2\pi l\text{n}}{\lambda} \quad (25)$$

where Δ is the phase variation in radians, l is the propagation distance, n is the refractive index of the propagation medium, and λ is the wavelength of the light in *vacuo*. Δ for each of the propagating beams depicted in Figure 1 can be calculated from the geometry of the system and are given in Appendix A.

(D) Model Parameters. Appropriate values for some of the variables needed for the SF calculations are easy to select; others are specific to the chosen substrate materials and require more critical appraisal (Table 1). Although in principle, the calculations can be applied to many combinations of dielectric and metal it is useful to choose a realistic pair of materials to generate representative quantitative results. In this work, calculations have been completed for a composite substrate composed of mica and gold. Mica is an ideal dielectric material to consider for this application as it can be cleaved to provide atomically smooth sheets micrometers in thickness.

The refractive index of the transmitting medium is an important factor in the distance/phase relationship function. In contrast to the well-known real and imaginary refractive index

Interference Effects in Sum Frequency Spectra

J. Phys. Chem. B, Vol. 106, No. 21, 2002 **5465**

components of metals[33] (e.g., gold), those of dielectrics (e.g., mica) are less well defined and where published, typically relate only to real components and the visible region of the spectrum.[34-38] However, from the work of El-Zaiat,[35] the refractive index averages used here of $n_{2,\text{VIS}} = 1.60$ and $n_{2,\text{SF}} = 1.63$ were derived. Singleton and Shirkey[39] measured both real and imaginary refractive index components of mica between 400 and 1200 cm^{-1}. The reported values change significantly over this range and the rather long extrapolation into the C−H stretching region where the SF spectra of interest in this study are generated (2800 − 3000 cm^{-1}) is therefore unreliable. To circumvent this potential difficulty, the refractive index in this region was measured in this work by analyzing the Fabry−Perot interference fringes generated in the linear-infrared transmission spectrum of thin mica sheets of different thickness[10,40] to yield an average real refractive index component of $n_{2,\text{IR}} = 1.65 \pm 0.03$ between 2800 and 3000 cm^{-1}. Although suitable real components of the refractive index were available or determinable, it was not possible to obtain imaginary components. The imaginary components, both in the visible and the infrared, have therefore been set to zero. This assumption is not expected to lead to significant discrepancies in the modeling results when considering mica sheets only micrometers in thickness.

The composite substrate model contains several parameters only pertinent to the hydrocarbon chain molecules adsorbed at the air/dielectric interface. These are the effective refractive index of the monolayer, n_{layer}, the tilt angle of the chain to the surface normal κ, and the ratio R of the hyperpolarizabilities, $\beta_{\text{aac}}/\beta_{\text{ccc}}$. The refractive index of a layer of terminal methyl groups or of a monolayer is conceptually difficult to define because refractive index is inherently a bulk property relative to the wavelength of light. A common assumption in published SF studies is that the monolayer refractive index equals that of one of the confining bulk media,[41-44] whereas in others it, has been equated to the bulk refractive index of the monolayer material itself.[42,45] No consensus has been reached and the values quoted for a densely packed hydrocarbon monolayer fall in a broad range from 1.45 to 3.5. Recently, Zhuang et al.[23] reviewed the n_{layer} values cited in the literature for hydrocarbon monolayers and concluded that $n_{\text{layer(methyl)}} = 1.18$. This value has been adopted in the present work. Although it is rather lower than the generally accepted bulk value for hydrocarbons of 1.45,[42] the terminal methyl groups of the monolayer are in contact with air and n_{layer} may be expected to be considerably altered from the bulk value. Although, in principle, a value of R can be obtained from the Raman depolarization ratio this has not been reported in the literature and so the value of $R = 2.5$ calculated by Zhuang et al.[23] for a densely packed hydrocarbon monolayer has been adopted. The value of the tilt angle used, $\kappa = 21 \pm 4°$, is based on X-ray reflectivity[46] and diffraction[47] data of octadecylsiloxane (ODS) monolayers. This value is compatible with theoretical predictions made on the same monolayer system of 15 to 20° by Finklea et al.[48] and SFS results of $25 \pm 2°$ by Löbau et al.[49] The value of $\xi = 34.5°$ is taken from Lide's microwave spectroscopy work on propane in the gas phase.[50]

Results and Discussion

Simulations Overview. The SF relative intensity simulations were completed using a Mathematica[51] program (Supporting Information) based on the equations of the calculation section. The interference effects arise from the complex nature of the electric dipole terms and it is therefore instructive

to expand eq 1 in polar form

$$I_{i,\text{SF}} = |\mathbf{E}_{i,\text{SF}}^{\text{Total}}|^2$$

$$= |\mathbf{E}_{i,\text{SF1}} + \mathbf{E}_{i,\text{SF2}} + \mathbf{E}_{i,\text{SF3}}|^2$$

$$= |\mathbf{E}_{i,\text{SF1}}|^2 + |\mathbf{E}_{i,\text{SF2}}|^2 + |\mathbf{E}_{i,\text{SF3}}|^2 + 2|\mathbf{E}_{i,\text{SF1}}||\mathbf{E}_{i,\text{SF2}}|\cos\Pi + 2|\mathbf{E}_{i,\text{SF1}}||\mathbf{E}_{i,\text{SF3}}|\cos\Omega + 2|\mathbf{E}_{i,\text{SF2}}||\mathbf{E}_{i,\text{SF3}}|\cos\Psi \quad (26)$$

Equation 26 illustrates that the SF signal can be described using three single terms ($|\mathbf{E}_{i,\text{SF1}}|^2$, $|\mathbf{E}_{i,\text{SF2}}|^2$ and $|\mathbf{E}_{i,\text{SF3}}|^2$) and three cross-terms. The latter include a trigonometric factor to describe the phase difference between the two components of each cross-term. Two conclusions can be drawn from eq 26 regarding the SF light incident on the experimental detector. First, the single resonant SF components, $|\mathbf{E}_{i,\text{SF1}}|^2$ and $|\mathbf{E}_{i,\text{SF2}}|^2$, will vary in magnitude with wavenumber (due to the nonlinear susceptibilities describing the resonant SF response) but not with dielectric thickness as this affects purely phase, and only produces a corresponding magnitude change in a cross-term. However, the resonant SF signal from a monolayer on a dielectric surface is particularly weak and both $|\mathbf{E}_{i,\text{SF1}}|^2$ and $|\mathbf{E}_{i,\text{SF2}}|^2$ are therefore likely to be negligible in comparison to $|\mathbf{E}_{i,\text{SF3}}|^2$ and the cross-terms. Second, the independent SF term $|\mathbf{E}_{i,\text{SF3}}|^2$ provides a SF signal invariant in both IR wavenumber and dielectric thickness and hence a featureless spectral baseline, offset from zero. The resonant spectral line-shape will appear superimposed on this baseline and be a convolution of the SF intensity generated by the three cross-term components, each of which will vary as a function of both IR wavenumber and dielectric thickness. Finally, although the electric field terms of eq 26 are dependent upon the Cartesian axis under consideration, the phase differences of each cross-term (Π, Ω, Ψ) are independent of axis choice. The SF intensities calculated along each of the Cartesian axes ($I_{i,\text{SF}}$) will therefore exhibit the same three thickness dependent interference components, but with differing relative magnitudes.

Model Results for the r^+ Resonance. The first simulation performed (not shown) was for zero thickness of the dielectric material in order to provide an initial spectrum devoid of thickness/phase effects. The value of ϵ (the SF phase offset of the metal layer, eq 10) employed in the simulation was subsequently modified to a value of 169° to provide agreement between the line-shape observed in the zero thickness simulation and that obtained empirically from a hydrocarbon chain adsorbed directly on gold[8] (for a counter-propagating beam geometry and the experimental variables in Table 1). Preliminary simulations of the r^+ composite substrate spectrum at dielectric thicknesses of 1 and 2 μm confirmed that the spectral line-shape varied significantly with thickness. To obtain a comprehensive picture of the periodic nature of the interference effect the SF intensity is plotted as a function of the infrared wavenumber and the dielectric thickness, d, in Figure 2. Further analysis was completed using a 2D plot of the normalized SF intensity on resonance ($\omega_V = \omega_{\text{IR}}$) as a function of the dielectric thickness, Figure 3a. Intensities less than unity correspond to dips and intensities greater than unity to peaks in the SF spectra. It can be seen from Figure 3a that the dominant periodicity occurs at $\sim$3 μm; a lower intensity periodicity (of $\sim$160 nm) is superimposed upon it. The periodicity and intensity of the two contributions is unchanged with dielectric thickness, as expected because only real refractive index components are used. It should be noted that the maximum intensity of a resonant peak (e.g., for $d = 3$ μm, $I_{\text{SF}} \approx 1.3$, $\Delta I_{\text{SF}} \approx 0.3$) is greater than the maximum decrease of a resonant dip (e.g., for $d = 1.5$ μm, I_{SF}
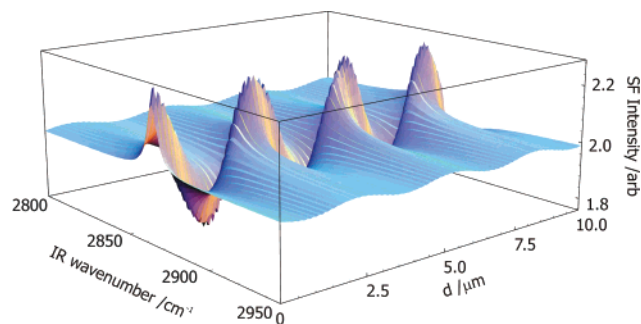
Figure 2. Topographical plot of the SF intensity as a function of the infrared wavenumber and the thickness of the dielectric material, *d*, for the r^+ vibrational mode and the ppp beam polarization combination.
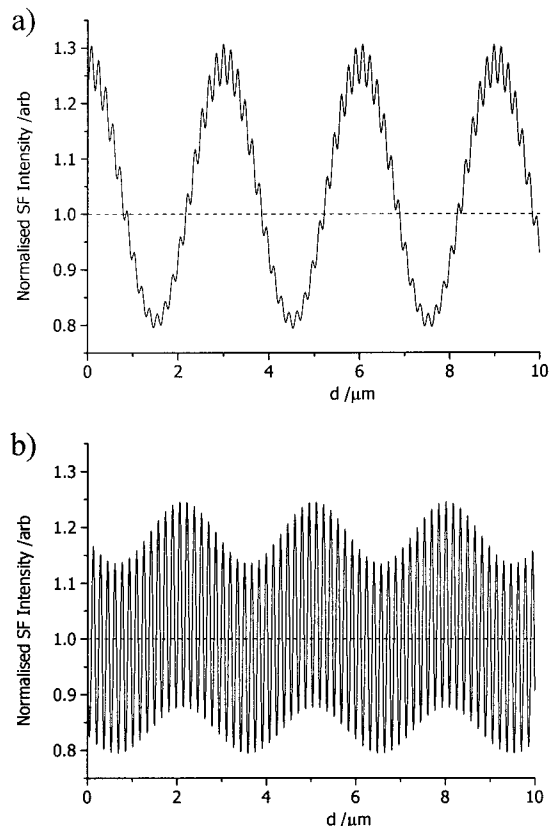

Figure 3. Normalized SF intensity of (a) the r^+ vibrational mode on resonance (2878 cm^{-1}) and (b) the r^- vibrational mode on resonance (2966 cm^{-1}) as function of the thickness of the dielectric material, *d*, for the ppp beam polarization combination.

≈ 0.8, $\Delta I_{SF} \approx 0.2$). This arises because the simulated SF intensity is proportional to the square of the surface SF E field.

Although the simulation of Figure 3a appears to predict only two dielectric thickness/phase contributions, a Fourier transform of the data of Figure 3a identifies a third weak component with a periodicity of ~150 nm (~6.65 oscillations per μm), Figure 4a. The three components evident in Figure 4a arise from the three cross-terms of eq 26, with the two more intense components attributable to cross-terms involving the SF signal from the metal surface (SF1/SF3 and SF2/SF3) and the weak component arising from SF1/SF2. Confirmation of these assignments follows from considering the three cross-terms present in eq 26 individually. Considering the SF1/SF3 cross-term first

$$2|\mathbf{E}_{i,SF1}||\mathbf{E}_{i,SF3}|\cos\Omega \qquad (27)$$

and expanding Ω, the phase difference between SF1 and SF3
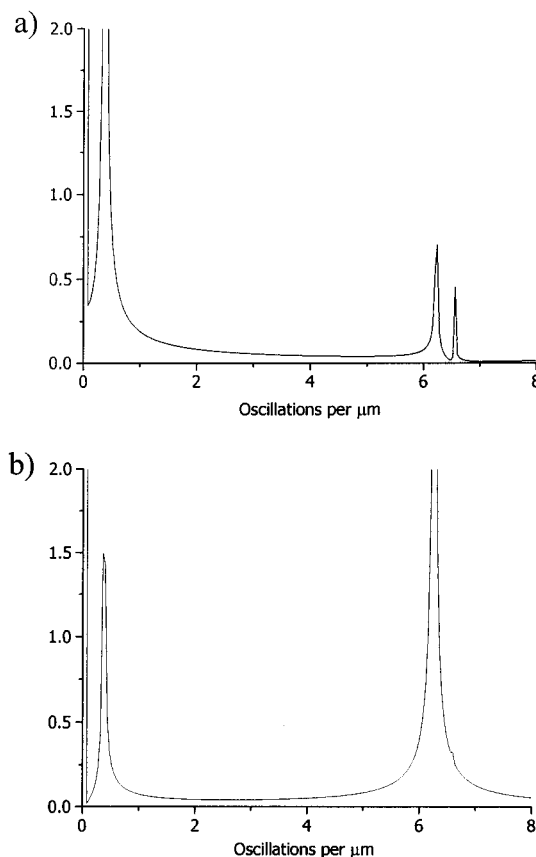

Figure 4. Fourier transforms of the simulations depicted in Figure 3 indicating that (a) there are three unique frequency contributions to the normalized SF intensity of the r^+ vibrational mode and (b) that there are only two significant frequency components of the r^- vibrational mode.

as a function of both the IR wavenumber and dielectric thickness gives

$$2|\mathbf{E}_{i,SF1}||\mathbf{E}_{i,SF3}|\cos[(\epsilon + \Delta_{SF3}^{Total}(d)) - (\delta(\omega_{IR}) + \Delta_{SF1}^{Total}(d))] \qquad (28)$$

where ϵ is the phase offset of the SF signal generated at the metal surface (169°), $\delta(\omega_{IR})$ is the wavelength-dependent phase due to the nonlinear susceptibilities ($\chi_{ijk}^{(2)}$) and $\Delta_{SF1}^{Total}(d)$, $\Delta_{SF3}^{Total}(d)$ represent the combined thickness/phase equations generated by summation of the individual thickness/phase functions given in Appendix A. Equation 28 shows that the total dielectric thickness/phase response of the cross-term is dependent upon the *difference* between the thickness/phase variation of the separate beams, specifically $\Delta_{SF3}^{Total}(d) - \Delta_{SF1}^{Total}(d)$.

The dielectric thickness/phase variations for the individual SF beams are calculated to be

$$\Delta_{SF1}^{Total}(d) = 645.47°/\mu m \qquad (29)$$

$$\Delta_{SF2}^{Total}(d) = 2991.10°/\mu m \qquad (30)$$

$$\Delta_{SF3}^{Total}(d) = 2871.53°/\mu m \qquad (31)$$

The phase change per unit distance for the SF1 beam which propagates through air is more gradual than for the SF2 and SF3 beams which pass through the dielectric medium. For the SF1/SF3 cross-term the calculated phase change per micrometer is 2226° i.e., a periodicity of 162 nm. For the SF2/SF3 cross-
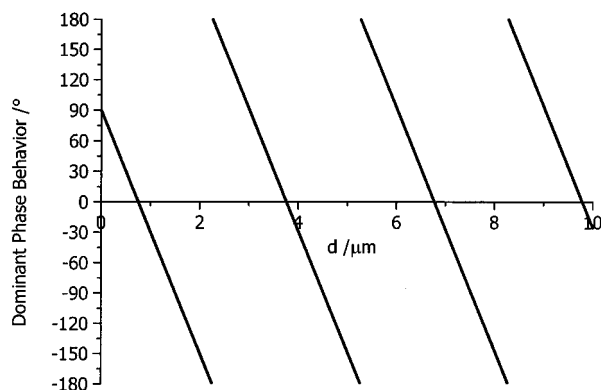
Interference Effects in Sum Frequency Spectra

J. Phys. Chem. B, Vol. 106, No. 21, 2002 **5467**

Figure 5. Predicted dielectric thickness/phase behavior of the r^+ vibrational mode on resonance probed by the ppp beam polarization combination. Calculated employing the dominant SF2/SF3 cross-term periodicity of 3.01 μm.

term the equivalent periodicity is calculated to be 3.01 μm and for the SF1/SF2 cross-term the value is 153 nm. These values concur with those of Figure 4a. A diagrammatic representation of the dielectric thickness/phase relationship for the dominant SF2/SF3 cross-term is given in Figure 5.

The dominance of the SF2/SF3 cross-term over the other cross-terms is attributed to the fact that the x and z intensity components of the SF2 and SF3 beams are in phase, Figure 6a, whereas for example the same components of the SF1 and SF3 beams are out of phase, Figure 6b. Consequently, the net cross-term intensity which is the sum of the individual components at each thickness value is minimal for SF1/SF3 and substantial for SF2/SF3. The intensity difference between the x

and z components in Figure 6 arises from the differing magnitudes of the component susceptibilities (i.e., z components generated by $\chi^{(2)}_{zzz}$ and $\chi^{(2)}_{zxx}$, x components by $\chi^{(2)}_{xzx}$ and $\chi^{(2)}_{xxz}$). The observed phase difference between the x and z components is attributed to the nonlinear Fresnel factors. For SF2/SF3, L^T_x and L^T_z are both positive but for SF1/SF3 L^R_x and L^R_z have opposite signs and generate E fields which are out of phase.

It was found that a variation of $\pm$ 0.1 in the values of the three refractive indices of the dielectric ($n_{2,SF}$, $n_{2,VIS}$, and $n_{2,IR}$) produced only a 0.2 μm variation in the periodicity of the dielectric thickness/phase relationship of the SF2/SF3 cross-term, a comparatively minor effect. The values of $n_{2,SF}$ and $n_{2,VIS}$ for the simulation are accurate to better than $\pm$ 0.02, and although $n_{2,IR}$ is less accurately known, its uncertainty is likely to be within $\pm$ 0.1. Hence, inaccuracies in the modeling results due to the values of the refractive indices employed are minor.

The calculations have been made for incident laser beam angles of 60 and 65° to the surface normal for the visible and infrared beams, respectively. Changes in these angles will affect both the Fresnel factors and the phase/distance relationships; consequently, the predicted intensities and periodicities would be expected to be modified. In an actual SF experiment, beam angles are typically controlled to better than 0.5°. Simulations showed that variations of 3° in the incident beam angles were required before significant intensity and periodicity variations were detectable.

The three parameters relating to a specific monolayer film, κ, R and n_{layer}, only appear in the susceptibility equations and their associated uncertainties therefore only affect the relative intensities of the dielectric thickness/phase components. A
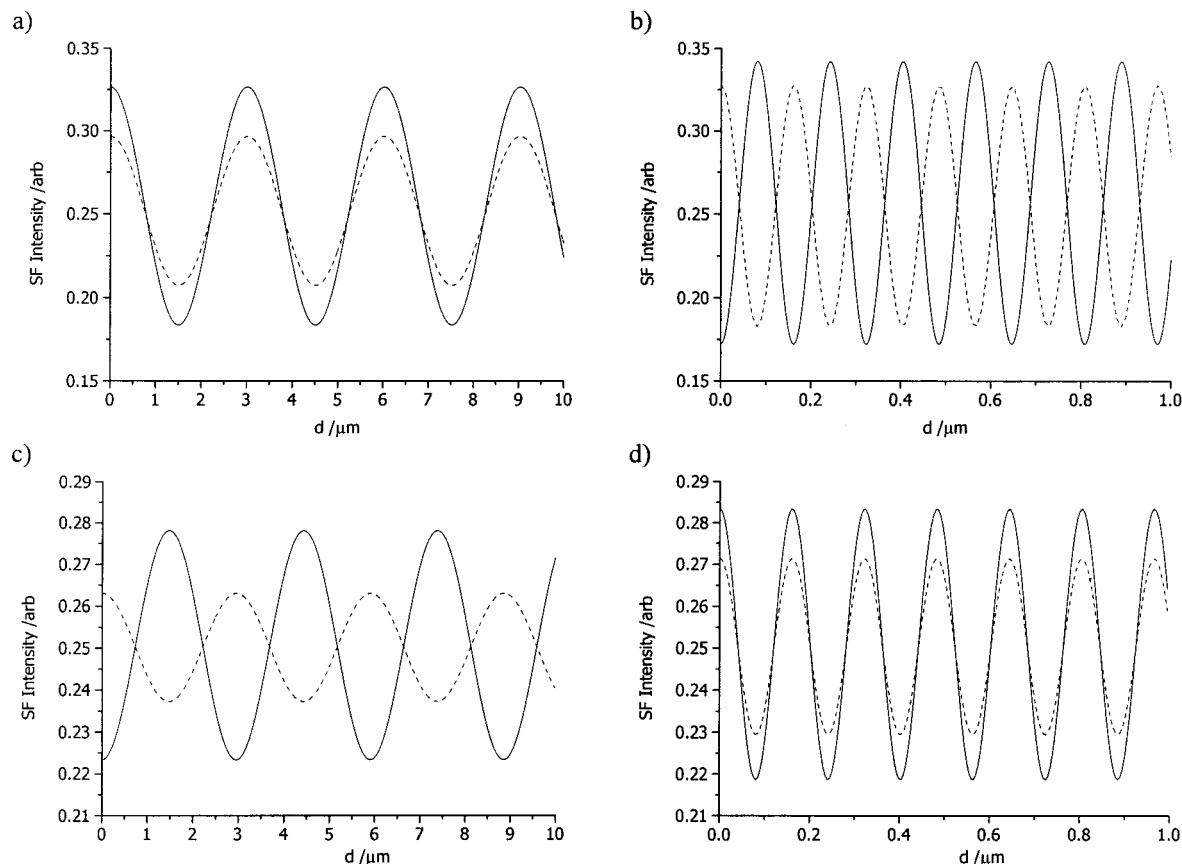

Figure 6. x and z axis components (solid and broken lines respectively) of the SF intensity for (a) the SF2/SF3 cross-term of the r^+ mode on resonance, (b) the SF1/SF3 cross-term of the r^+ mode on resonance, (c) the SF2/SF3 cross-term of the r^- mode on resonance and (d) the SF1/SF3 cross-term of the r^- mode on resonance. All calculations refer to the ppp beam polarization combination.

variation of ± 10° in κ (i.e., κ = 11, 21, and 31°) had a negligible affect on the interference spectrum. In contrast, variations in R of ± 1 and changes in the value of n_{layer}, from 1.45 to 3.5 produced significant affects on the simulations.

Model Results for the r^- Resonance. Because the theoretical model used to predict the dielectric thickness/phase behavior of the r^- resonance differs only marginally from that for the r^+ resonance it is not presented in detail. All the input parameters are the same as in Table 1, except ω_v which is set to 2966 cm^{-1}. The resulting r^- normalized dielectric thickness/intensity plot on resonance is given in Figure 3b. An obvious conclusion is that a substantial variation in the relative importance of the individual SF cross-terms occurs in comparison to the r^+ simulation. The SF1/SF3 cross-term dominates the simulation and a net rapid dielectric thickness/phase change occurs, modulated by a weaker and longer SF2/SF3 contribution. The Fourier transform of the data, Figure 4b, confirms that the periodicities of the SF1/SF3 and SF2/SF3 cross-terms are unchanged from the r^+ simulation although their relative intensities are reversed. The SF1/SF2 component with a dielectric thickness/phase periodicity of 152 nm which was present in the r^+ Fourier transform spectrum (Figure 4a) is obscured by the SF1/SF3 cross-term.

To elucidate the origin of the differences in the r^+ and r^- model predictions (Figure 3) the individual x and z components of the SF1/SF3 and SF2/SF3 cross-terms are plotted in Figure 6. The x and z components of the SF2/SF3 cross-term, Figure 6c, are out of phase, whereas for the SF1/SF3 cross-term (Figure 6d) they are in phase, the reverse of the situation for the r^+ resonance. It arises due to the sign differences of the r^+ and r^- susceptibility equations and accounts for the dominance of the SF1/SF3 over the SF2/SF3 cross-term in Figure 3b. A second feature of the simulations is that the phase variations in the SF2/SF3 x and z components are responsible for a 180° phase shift in the periodicity of the net SF intensity arising from the cross-term. This manifests itself in a subtle way in Figure 3b. The larger periodicity component is a minimum at 0 μm and a maximum at 1.5 μm, exactly opposite that of the simulation of Figure 3a. The same shift does not occur in the SF1/SF3 cross-term and because this dominates the simulation of the r^- resonance mode a peak is still predicted to appear at 0 μm.

Model Results for r^+ and r^- Resonances in the ssp Beam Polarization Combination. Interpretation of the simulated ssp beam polarization predictions is simpler than for the ppp polarization because only one E field need be considered for each of the three SF cross-terms. Note that in a manner similar to that performed for the ppp simulations, the value of ϵ was set to 0° so that the line-shape obtained in a zero thickness simulation matched that obtained empirically. The model predictions for the r^+ and r^- methyl resonances are shown in Figure 7. It is evident for both the r^+ and r^- resonances that equal intensity contributions are predicted from the SF1/SF3 and SF2/SF3 cross-terms. The net result is a dielectric thickness/phase effect of short periodicity modulated by an equally intense longer periodicity. However, due to the differing susceptibility equations used for the resonances the intensity variation for the r^+ resonance is considerably larger than for the r^- resonance (as expected the actual periodicities are unchanged from the ppp beam polarization predictions).

Concluding Remarks

The composite substrate technique is capable of providing substantial SF signal enhancements from a monolayer adsorbed on a dielectric surface, as demonstrated by our recent
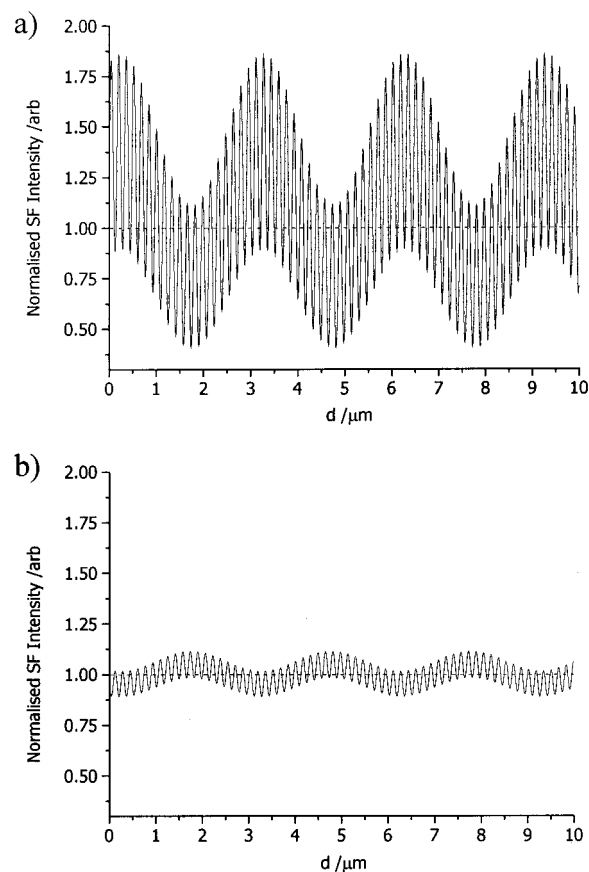

Figure 7. Normalized SF intensity of (a) the r$^+$ vibrational mode on resonance (2878 cm^{-1}) and (b) the r^- vibrational mode on resonance (2966 cm^{-1}) as function of the thickness of the dielectric material, d, for the ssp beam polarization combination.

publication of the first successful experimental investigation to utilize the principle.[15] The current work has considered the theoretical aspects of the composite substrate and has predicted the relationship between the line-shapes observed in the experimental SF spectra and the thickness of the dielectric material. The SF signal emitted is found to be dominated by the cross-terms between resonant and nonresonant sources of SF radiation. These two sources are physically separated from each other and coherently interfere. Each cross-term has a characteristic phase periodicity as the thickness of the dielectric layer changes. The first cross-term, SF1/SF3, encompasses the resonant SF signal generated at the dielectric/air interface (where the monolayer resides) that transmits into air (SF1), and the nonresonant SF signal generated at the dielectric/metal interface (SF3). The second cross-term (SF2/SF3) contains the resonant SF signal generated at the dielectric/air interface that transmits into the dielectric (SF2) and the nonresonant SF signal, SF3. The model predicts that for the ppp beam polarization combination the phase periodicity of the r^+ resonance is predominantly 3.01 μm, whereas for the r^- resonance it is 162 nm. This arises because one or other of the cross-terms is dominant and each has a markedly different periodicity. In contrast, the ssp polarization combination is predicted to produce an SF response containing both short and long phase periodicities of approximately equal magnitude for both r^+ and r^- resonances. This is because both cross-terms have equal weighting in these cases. The theoretical predictions presented in this work are compared to an empirical determination of the dielectric thickness/line-shape behavior in a future publication.

Interference Effects in Sum Frequency Spectra

J. Phys. Chem. B, Vol. 106, No. 21, 2002 **5469**

Appendix A: Phase Variations, Δ's, of the Sum Frequency, Infrared and Visible Beams of the Dielectric/Metal Composite Substrate

The geometry of the system is that of Figure 1 with the addition of the angles defined below
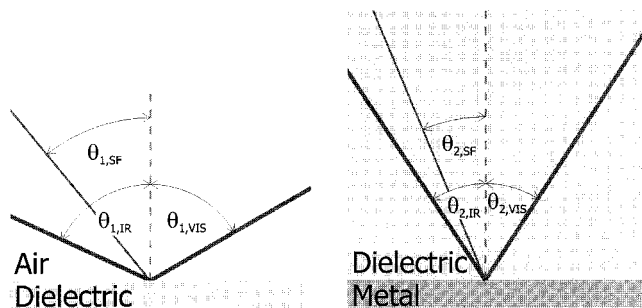
$$\Delta_{\text{SF1}} = 0 \tag{A.1}$$

$$\Delta_{\text{IR1}} = \frac{2\pi n_{1,\text{IR}}}{\lambda_{\text{IR}}} d[\tan\theta_{2,\text{IR}} - \tan\theta_{2,\text{SF}}]\sin\theta_{1,\text{IR}} \tag{A.2}$$

$$\Delta_{\text{VIS1}} = \frac{2\pi n_{1,\text{VIS}}}{\lambda_{\text{VIS}}} d[\tan\theta_{2,\text{VIS}} + \tan\theta_{2,\text{SF}}]\sin\theta_{1,\text{VIS}} \tag{A.3}$$

$$\Delta_{\text{SF2}} = \frac{2\pi n_{2,\text{SF}}}{\lambda_{\text{SF}}} \frac{2d}{\cos\theta_{2,\text{SF}}} \tag{A.4}$$

$$\Delta_{\text{IR2}} = \frac{2\pi n_{1,\text{IR}}}{\lambda_{\text{IR}}} d[\tan\theta_{2,\text{IR}} + \tan\theta_{2,\text{SF}}]\sin\theta_{1,\text{IR}} \tag{A.5}$$

$$\Delta_{\text{VIS2}} = \frac{2\pi n_{1,\text{VIS}}}{\lambda_{\text{VIS}}} d[\tan\theta_{2,\text{VIS}} - \tan\theta_{2,\text{SF}}]\sin\theta_{1,\text{VIS}} \tag{A.6}$$

$$\Delta_{\text{SF3}} = \frac{2\pi n_{2,\text{SF}}}{\lambda_{\text{SF}}} \frac{d}{\cos\theta_{2,\text{SF}}} \tag{A.7}$$

$$\Delta_{\text{IR3}} = \frac{2\pi n_{2,\text{IR}}}{\lambda_{\text{IR}}} \frac{d}{\cos\theta_{2,\text{IR}}} \tag{A.8}$$

$$\Delta_{\text{VIS3}} = \frac{2\pi n_{2,\text{VIS}}}{\lambda_{\text{VIS}}} \frac{d}{\cos\theta_{2,\text{VIS}}} \tag{A.9}$$

Supporting Information Available: The Mathematica code listing for the composite structure model. This material is available free of charge via the Internet at http://pubs.acs.org.

References and Notes

(1) Shen, Y. R. *Nature* **1989**, *337*, 519−525.
(2) Bain, C. D. *J. Chem. Soc.-Faraday Trans.* **1995**, *91*, 1281−1296.
(3) Miranda, P. B.; Shen, Y. R. *J. Phys. Chem. B* **1999**, *103*, 3292−3307.
(4) Eisenthal, K. B. *Chem. Rev.* **1996**, *96*, 1343−1360.
(5) Messmer, M. C.; Conboy, J. C.; Richmond, G. L. *J. Am. Chem. Soc.* **1995**, *117*, 8039−8040.
(6) Conboy, J. C.; Messmer, M. C.; Richmond, G. L. *J. Phys. Chem.* **1996**, *100*, 7617−7622.
(7) Bloembergen, N.; Pershan, P. S. *Phys. Rev.* **1962**, *128*, 606.
(8) Bain, C. D.; Davies, P. B.; Ong, T. H.; Ward, R. N.; Brown, M. A. *Langmuir* **1991**, *7*, 1563−1566.
(9) Ward, R. N.; Davies, P. B.; Bain, C. D. *J. Phys. Chem.* **1993**, *97*, 7141−7143.
(10) Lambert, A. G. Ph.D. Thesis, University of Cambridge, 2001.
(11) Evans, S. D.; Sharma, R.; Ulman, A. *Langmuir* **1991**, *7*, 156−161.
(12) Laibinis, P. E.; Bain, C. D.; Nuzzo, R. G.; Whitesides, G. M. *J. Phys. Chem.* **1995**, *99*, 7663−7676.
(13) Sprik, M.; Delamarche, E.; Michel, B.; Rothlisberger, U.; Klein, M. L.; Wolf, H.; Ringsdorf, H. *Langmuir* **1994**, *10*, 4116−4130.
(14) Ong, T. H.; Davies, P. B.; Bain, C. D. *Langmuir* **1993**, *9*, 1836−1845.
(15) Lambert, A. G.; Neivandt, D. J.; McAloney, R. A.; Davies, P. B. *Langmuir* **2000**, *16*, 8377−8382.
(16) Briggs, A. M.; Usadi, E. W.; Davies, P. B. *Abstr. Pap. Am. Chem. Soc.* **1997**, *214*, 286-PHYS.
(17) Shen, Y. R. *The Principles of Nonlinear Optics*; Wiley: New York, 1984.
(18) Hirose, C.; Akamatsu, N.; Domen, K. *J. Chem. Phys.* **1992**, *96*, 997−1004.
(19) Hirose, C.; Akamatsu, N.; Domen, K. *Appl. Spectrosc.* **1992**, *46*, 1051−1072.
(20) Hirose, C.; Yamamoto, H.; Akamatsu, N.; Domen, K. *J. Phys. Chem.* **1993**, *97*, 10 064−10 069.
(21) Hirose, C.; Ishida, H.; Iwatsu, K.; Watanabe, N.; Kubota, J.; Wada, A.; Domen, K. *J. Chem. Phys.* **1998**, *108*, 5948−5956.
(22) Ishida, H.; Iwatsu, K.; Kubota, J.; Wada, A.; Domen, K.; Hirose, C. *J. Chem. Phys.* **1998**, *108*, 5957−5964.
(23) Zhuang, X.; Miranda, P. B.; Kim, D.; Shen, Y. R. *Phys. Rev. B* **1999**, *59*, 12 632−12 640.
(24) Bell, G. R.; Bain, C. D.; Ward, R. N. *J. Chem. Soc.-Faraday Trans.* **1996**, *92*, 515−523.
(25) Watanabe, N.; Yamamoto, H.; Wada, A.; Domen, K.; Hirose, C.; Ohtake, T.; Mino, N. *Spectroc. Acta Pt. A-Molec. Biomolec. Spectrosc.* **1994**, *50*, 1529−1537.
(26) Braun, R.; Casson, B. D.; Bain, C. D.; van der Ham, E. W. M.; Vrehen, Q. H. F.; Eliel, E. R.; Briggs, A. M.; Davies, P. B. *J. Chem. Phys.* **1999**, *110*, 4634−4640.
(27) Duffy, D. C. Ph.D. Thesis, University of Cambridge, 1996.
(28) Liebsch, A. *Appl. Phys. B−Lasers Opt.* **1999**, *68*, 301−304.
(29) Maytorena, J. A.; Mendoza, B. S.; Mochan, W. L. *Phys. Rev. B* **1998**, *57*, 2569−2579.
(30) Mendoza, B. S.; Mochan, W. L.; Maytorena, J. A. *Phys. Rev. B* **1999**, *60*, 14 334−14 340.
(31) Heinz, T. F. Ph.D. Thesis, Appendix I, University of California, 1982.
(32) Braun, R.; Casson, B. D.; Bain, C. D. *Chem. Phys. Lett.* **1995**, *245*, 326−334.
(33) Palik, E. D. *Handbook of Optical Constants of Solids*; Academic Press Inc.: Orlando, 1985.
(34) Khashan, M. A.; Nassif, A. Y. *J. Mod. Opt.* **1989**, *36*, 785−796.
(35) El-Zaiat, S. Y. *Opt. Laser Technol.* **1997**, *29*, 495−500.
(36) Bailey, A. I.; Kay, S. M. *Brit. J. Appl. Phys.* **1965**, *16*, 39.
(37) Khashan, M. A. *Optica Acta* **1979**, *26*, 881.
(38) Faust, R. C. *Proc. Phys. Soc. B* **1952**, *65*, 48.
(39) Singleton, E. B.; Shirkey, C. T. *Appl. Optics* **1983**, *22*, 185−189.
(40) Guzonas, D. A.; Hair, M. L.; Tripp, C. P. *Appl. Spectrosc.* **1990**, *44*, 290−293.
(41) Berkovic, G.; Rasing, T.; Shen, Y. R. *J. Opt. Soc. Am. B−Opt. Phys.* **1987**, *4*, 945−949.
(42) Zhang, T. G.; Zhang, C. H.; Wong, G. K. *J. Opt. Soc. Am. B−Opt. Phys.* **1990**, *7*, 902−907.
(43) Zhuang, X.; Wilk, D.; Marrucci, L.; Shen, Y. R. *Phys. Rev. Lett.* **1995**, *75*, 2144−2147.
(44) Heinz, T. F.; Tom, H. W. K.; Shen, Y. R. *Phys. Rev. A* **1983**, *28*, 1883−1885.
(45) Johal, M. S.; Usadi, E. W.; Davies, P. B. *J. Chem. Soc.-Faraday Trans.* **1996**, *92*, 573−578.
(46) Wasserman, S. R.; Whitesides, G. M.; Tidswell, I. M.; Ocko, B. M.; Pershan, P. S.; Axe, J. D. *J. Am. Chem. Soc.* **1989**, *111*, 5852−5861.
(47) Tidswell, I. M.; Rabedeau, T. A.; Pershan, P. S.; Kosowsky, S. D.; Folkers, J. P.; Whitesides, G. M. *J. Chem. Phys.* **1991**, *95*, 2854−2861.
(48) Finklea, H. O.; Robinson, L. R.; Blackburn, A.; Richter, B.; Allara, D.; Bright, T. *Langmuir* **1986**, *2*, 239−244.
(49) Lobau, J.; Rumphorst, A.; Galla, K.; Seeger, S.; Wolfrum, K. *Thin Solid Films* **1996**, *289*, 272−281.
(50) Lide, D. R. *J. Chem. Phys.* **1960**, *33*, 1514−1518.
(51) Mathematica, Version 3.0, Wolfram Research, Inc., 1988−1996.